Wiley
Journal of Food Biochemistry
Volume 2024, Article ID 2919608, 17 pages
https://doi.org/10.1155/jfbc/2919608

WILEY

Research Article

Fluorescence Labeling to Study the Distribution of *Radix Puerariae lobatae* Polysaccharide in Cells and Mice

Wen Cao,[1,2,3] **Qiuyue Lv**,[1,2,3,4] **Xin Zhan**,[1,2,3] **Shihan He**,[1,2,3] **Jie Yu**,[1,2,3] **Zhu Yang**,[1,2,3] **Guodong Wang**,[1,2,3,4] **Jiangping Wu**,[1,2,3,4] **and Jun Han**[1,2,3,4,5]

[1]*Center for Xin'an Medicine and Modernization of Traditional Chinese Medicine of IHM, Wannan Medical College, Wuhu 241002, China*
[2]*Anhui Provincial Engineering Laboratory for Screening and Re-Evaluation of Active Compounds of Herbal Medicines in Southern Anhui, Wannan Medical College, Wuhu 241002, China*
[3]*Anhui Provincial Engineering Research Center for Polysaccharide Drugs, Wannan Medical College, Wuhu 241002, China*
[4]*Anhui Innovative Center for Drug Basic Research of Metabolic Diseases, Wannan Medical College, Wuhu 241002, China*
[5]*Wuhu Modern Technology Research and Development Center of Chinese Herbal Medicine and Functional Food, Anhui College of Traditional Chinese Medicine, Wuhu 241002, China*

Correspondence should be addressed to Jiangping Wu; wujiangping09@126.com and Jun Han; hanjun@wnmc.edu.cn

Received 19 August 2024; Accepted 12 December 2024

Academic Editor: Xuelin Zhou

Copyright © 2024 Wen Cao et al. This is an open access article distributed under the Creative Commons Attribution License, which permits unrestricted use, distribution, and reproduction in any medium, provided the original work is properly cited.

Radix Puerariae lobatae polysaccharide (PLP1, M_w = 10.43 kDa), a novel polysaccharide isolated in our previous studies, possesses remarkable hepatoprotective properties. In this study, a highly sensitive fluorescent probe, namely, PLP1-tyrosine (TYR)-fluorescein isothiocyanate (FITC), was developed to investigate the distribution of PLP1 *in vitro* and *in vivo*. The fluorescent probe was characterized using fluorescence, high-performance gel permeation chromatography, infrared spectroscopy, ultraviolet spectroscopy, and nuclear magnetic resonance techniques, with a substitution degree of 0.53%. Toxicity assessments indicated that PLP1-TYR-FITC was nontoxic both *in vitro* and *in vivo*. *In vitro,* fluorescence microscopy revealed that PLP1-TYR-FITC may enter cells by endocytosis. *In vivo,* the distribution pattern of oral administration was as follows: small intestine > liver > kidney > spleen > stomach > heart > lung > brain. The distribution of intravenous administration was as follows: liver > small intestine > kidney > stomach > spleen > lung > heart > brain. FITC-labeled PLP1 was primarily distributed in the liver, supporting the hepatoprotective properties of PLP1. In summary, this study synthesized a PLP1 fluorescent probe to investigate PLP1 distribution *in vitro* and *in vivo*. Our findings lay the groundwork for further exploring the pharmacological mechanism of polysaccharides in *Pueraria lobata*.

Keywords: fluorescence labeling; *in vivo* imaging; pharmacokinetics; *pueraria lobata* polysaccharide; tissue distribution

1. Introduction

For generations, the dried root of *Pueraria lobata* (Willd.) Ohwi, also known as *Radix Pueraria lobata* belonging to the Fabaceae family, has been regarded as a vital component of traditional Chinese medicine in China, serving both medicinal and dietary purposes. Renowned for its anti-inflammatory, antioxidant, and immunomodulatory properties [1], *P. lobata* has been extensively applied in traditional medicine to address various diseases, such as liver injury and diabetes [2]. Previous studies have found that isoflavones and polysaccharides are the main chemical components of *P. lobata*, encouraging the application of *P. lobata* in traditional medicine [3].

Polysaccharides, natural polymers formed via the link between aldoses or ketoses via glycosidic bonds, are frequently administered for their immunostimulatory properties. Previous studies have reported diverse biological

functions of polysaccharides, including neuroprotective [4], anti-inflammatory [5], antioxidant [6], antiviral, antitumor [7], and hepatoprotective [8] properties. Moreover, a significant progress has been made in developing polysaccharide-based drugs, such as *Lentinus edodes* polysaccharide, which improves intestinal microecology [9]. However, despite their promising therapeutic potential, investigating the mechanisms of action and pharmacokinetics of polysaccharides is challenging due to their complex structure, large molecular weight, and absence of luminescent groups. Additionally, there is a dearth of direct and conclusive evidence supporting the ability of these biomacromolecules to bind to cells *in vitro* and affect the target organs *in vivo*. Furthermore, conventional analytical techniques, such as gas chromatography, mass spectrometry, and absorption spectrometry cannot effectively detect polysaccharides due to their high polarity and lack of luminescent groups, resulting in a significant gap between functional studies and studies on molecular mechanisms and metabolic kinetics [10, 11].

Currently, immunological methods, fluorescence labeling, and isotope labeling techniques are available methods for studying the *in vivo* pharmacokinetics of polysaccharides. Among them, fluorescent labeling and radioisotope labeling are the most commonly applied methods. Fluorescein isothiocyanate (FITC) is one of the most common fluorescent probes in fluorescence immunoassays due to its ease of experimental handling and high safety profile [12]. Additionally, fluorescent labeling significantly enhances the sensitivity of polysaccharide detection. Although FITC labeling of polysaccharides has been achieved for various substances, such as those from *Polygonatum sibiricum* [13], *Poria cocos* [14], and mulberry fruit [15], there is no report on fluorescent probes for *Pueraria lobata* polysaccharide.

Recently, our team isolated and identified a novel water-soluble polysaccharide from *Radix Pueraria lobata* in the Fanchang district of Wuhu City, naming it PLP1. Moreover, we revealed that PLP1 not only possesses greater free radical scavenging ability than amylose and amylopectin but also effectively regulates the expression of enzymes involved in alcohol metabolism, improves the antioxidant capacity, suppresses oxidative stress and inflammatory response, modulates lipid metabolism, prevents lipid accumulation, and positively regulates the intestinal flora to maintain intestinal homeostasis. Therefore, it can serve as a novel candidate drug for the clinical treatment of ALD. However, how to investigate the distribution of PLP1 *in vitro* and *in vivo* remains challenging. Leveraging the reductive terminal characteristic of PLP1, we facilitated the attachment of a secondary amino group to PLP1, which readily reacts with FITC. Subsequently, FITC was coupled with the reductive terminal of PLP1 to achieve fluorescent labeling. We measured the binding affinity of PLP1-TYR-FITC to HepG2 and AML12 cells and evaluated its distribution in mice after intragastric administration and intravenous injection. This study established a foundation to explore the clinical mechanisms underlying the beneficial effects of *P. lobata* polysaccharides.

2. Materials and Methods

2.1. Materials. *P. lobata* specimens were obtained from the Fanchang District of Wuhu City, Anhui Province, China. Professor Jun Han from Anhui College of Traditional Chinese Medicine in Wuhu, China, authenticated the materials, and a voucher specimen was deposited at the Herbarium of the College of Pharmaceutical Science, Wannan Medical College.

Ultraviolet (UV) and Fourier transform infrared (FT-IR) spectra were acquired using Shimadzu UV-2501 PC and FTIR-8400S spectrophotometers (Shimadzu, Kyoto, Japan), respectively. The Lc-l0Avp high-performance gel permeation chromatography (HPGPC) system (Shimadzu, Japan) was equipped with a RID-10 A refractive index detector. Single-dimensional NMR spectra were obtained using a Bruker AVANCE III 500 spectrometer (Karlsruhe, Germany) with D_2O as the solvent. Inverted fluorescence microscopy (Ts2R-FL, Japan) and a Small Animal Live Imager (IVIS Lumina LT∗, USA) were used for observation. DEAE-52 cellulose (2.5 × 40 cm), Sephadex G-75 dextran gels (1.6 × 60 cm), and chlorpromazine were purchased from Solarbio (Beijing, China). TYR, FITC, β-cyclodextrin, and sodium cyanine borohydride were purchased from Aladdin Reagent Co. The kits used to measure the concentrations of alanine aminotransferase (ALT), aspartate aminotransferase (AST), alkaline phosphatase (ALP), triglycerides (TGs), total cholesterol (TC), and creatinine (Crea) were purchased from Nanjing Jiancheng Institute of Biotechnology (Nanjing, China). All other reagents were of analytical grade, unless otherwise mentioned.

2.2. Preparation and Characterization of PLP1-TYR-FITC

2.2.1. Extraction and Purification of PLP1. PLP1 was extracted and purified using a previously published method [1]. Pretreated *P. lobata* powders were extracted three times at 95°C for 2 h each using hot water (10 mL/g). Subsequently, the powders were precipitated at 4°C using 4 volumes of 95% ethanol for 12 h. Using D101 macroporous resin and Sevag reagent, the extracts were then processed to remove pigments and proteins. The resulting crude polysaccharide products were dialyzed with distilled water (1 kDa, 48 h) and subsequently lyophilized. Finally, the crude polysaccharides were purified using DEAE-52 cellulose and Sephadex G-75 columns to obtain PLP1.

2.2.2. Preparation of PLP1-TYR. First, 200 mg of PLP1 was dissolved in 75 mL of PBS (0.2 mol/L, pH = 8.0). Subsequently, TYR (200 mg) and sodium cyanide borohydride (75 mg) were successively added to the reaction system. The resulting mixture was incubated at 37°C for 96 h with intermittent shaking. The supernatant was eliminated after centrifugation, and the precipitate was dissolved in ultrapure water. The eluate obtained was dialyzed for 48 h using deionized water and 1-kDa dialysis bags, followed by freeze-drying to derive the PLP1-TYR product. The product was kept in a desiccator.

2.2.3. Preparation of PLP1-TYR-FITC. After dissolving PLP1-TYR in ultrapure water, the pH of the solution was increased to 8.5 using sodium bicarbonate solution (0.5 mol/L). Thereafter, FITC was added and dark-incubated overnight at 37°C. Following the reaction, four volumes of absolute ethanol were added to induce precipitation, followed by centrifugation at 5000 r/min for 10 min. The supernatant was then discarded, and the precipitate was redissolved in ultrapure water. This process was repeated until the ethanol supernatant lost its fluorescence. Subsequently, the resulting precipitate was dissolved in ultrapure water and dialyzed using a 1-kDa dialysis bag for 48 h. Finally, PLP1-TYR-FITC was produced and kept in a light-free desiccator. Figure 1 depicts the labeling process of PLP1-TYR-FITC.

2.2.4. Characteristic Analysis of UV, FT-IR, and ^{1}H-NMR Spectra. PLP1 and PLP1-TYR-FITC were dissolved in deionized water to prepare 1 mg/mL solutions. Thereafter, they were scanned using a NanoDrop one Ultra-micro spectrophotometer (200–700 nm) to analyze UV characteristics (Thermo, USA). FT-IR spectra of PLP1 and PLP1-TYR-FITC were measured using a spectrometer (Nicolet iZ-10, Thermo Nicolet, USA). PLP1 and PLP1-TYR-FITC (2 mg each) were blended with KBr powder, and the resulting mixture was compressed into pellets for FT-IR analysis (4000-400 cm^{-1}) using Sanshu Biotech (Shanghai, China) [18]. Meanwhile, the ^{1}H-NMR spectra of PLP1 (D_2O), FITC (DMSO), and PLP1-TYR-FITC (D_2O) were obtained using a Bruker AVANCE NEO 500 M spectrometer, considering tetramethyl silane (TMS) as the internal control.

2.2.5. Excitation of Fluorescence and HPGPC Analysis. PLP1, FITC, and PLP1-TYR-FITC were suspended in distilled water to form 10 mg/mL solutions. The fluorescence intensities of the three samples were measured using a Duetta-Horiba Fluorescence and Absorbance spectrometer. Additionally, the homogeneity of PLP1 and PLP1-TYR-FITC was measured following our previous study. We used a Lc-l0Avp high-performance gel permeation chromatography (HPGPC) system (Shimadzu, Japan) equipped with an RID-10A refractive index detector. Following the standard elution protocol using a TSKgel G3000PWXL column (7.8 × 300 mm, Tosoh, Japan), we prepared 2 mg/mL PLP1 solution in deionized water, followed by HPGPC analysis. Deionized water served as the mobile phase (flow rate = 0.7 mL/min).

2.3. Quantification of Fluorescence Substitution. The centrifuge tubes were covered with foil paper, and all subsequent procedures were conducted in a dark environment. Precisely, 2 mg of FITC was weighed and combined with PBS (10 mL) to establish a FITC reference stock solution with a concentration of 200 μg/mL. The FITC stock solution was configured into 0.1, 0.5, 2.5, 10, 50, 100, 150, and 200 μg/mL gradient standard solutions. A blank control was established using an equal volume of PBS solution. The fluorescence intensities were measured under specific conditions (slit width = 2 nm, E_m = 525 nm, and E_x = 495 nm). Then, FITC standard curves were calibrated using β-cyclodextrin. Subsequently, standard curves were drawn based on the measurements, and the regression equation was determined. For further analysis, 1 mg of PLP1-TYR-FITC was dissolved in 10 mL of PBS. The fluorescence intensity was determined after vortex mixing to calculate the efficiency of fluorescence labeling for PLP1.

2.4. Cell Culture and Treatment. HepG2 and AML12 cells were provided by Saiku Biotechnology Ltd. Cell viability was determined using MTT assays. HepG2 and AML12 cells were seeded into 12-well plates at a density of 5×10^5 cells/well. They were cultured in a complete medium containing 10% bovine serum, MEM, and 1% nonessential amino acids. The experiment consisted of two groups. The first group was pretreated with the endocytosis inhibitor chlorpromazine (40 μM) for 30 min, while the second group was not treated. After removing the culture medium, both groups were incubated with PLP1-TYR-FITC (200 μg/mL) at 37°C in a 5% CO_2 incubator, protected from light, for 2 h. Subsequently, cells were rinsed three times with PBS. Next, 40 μL of antifluorescence quenching solution was added. The results were observed using fluorescence microscopy at 200x and 400x magnifications.

2.5. Animal and Experimental Design

2.5.1. Animals and Diet. SPF KM mice (weighing 18 ± 2 g) were provided by the Experimental Animal Center of Henan SkBys (Henan, China, SCXK(Yu)2020-0005) and maintained under specific pathogen-free conditions, with temperature and humidity of 22°C–25°C and 50%–55%, respectively. The laboratory food pellets and bedding were autoclaved, ensuring their sterility. Animals had unrestricted access to water and food under a 12 h light–dark cycle. This study was approved by the Laboratory of Animals Ethical Committee of Wannan Medical College and adhered to ARRIVE guidelines (WNMC-AWE-2023461).

2.5.2. Acute Toxicity Test. After 1 week of acclimatization, mice were randomly assigned to two groups: the normal group and the toxicity test group, with six mice in each group. The toxicity test group received a single gavage of PLP1-TYR-FITC solution (2000 mg/kg), whereas the normal group received an equivalent volume of saline. During the 14-day observation period, the physical appearance, mortality, and behavioral characteristics of all mice were recorded.

2.5.3. Subacute Toxicity Test. After 1 week of acclimatization, mice were randomly allocated to three groups: two drug groups (receiving 1000 and 2000 mg/kg of PLP1-TYR-FITC solution via gavage) and one normal group (receiving saline via gavage). Each group consisted of six

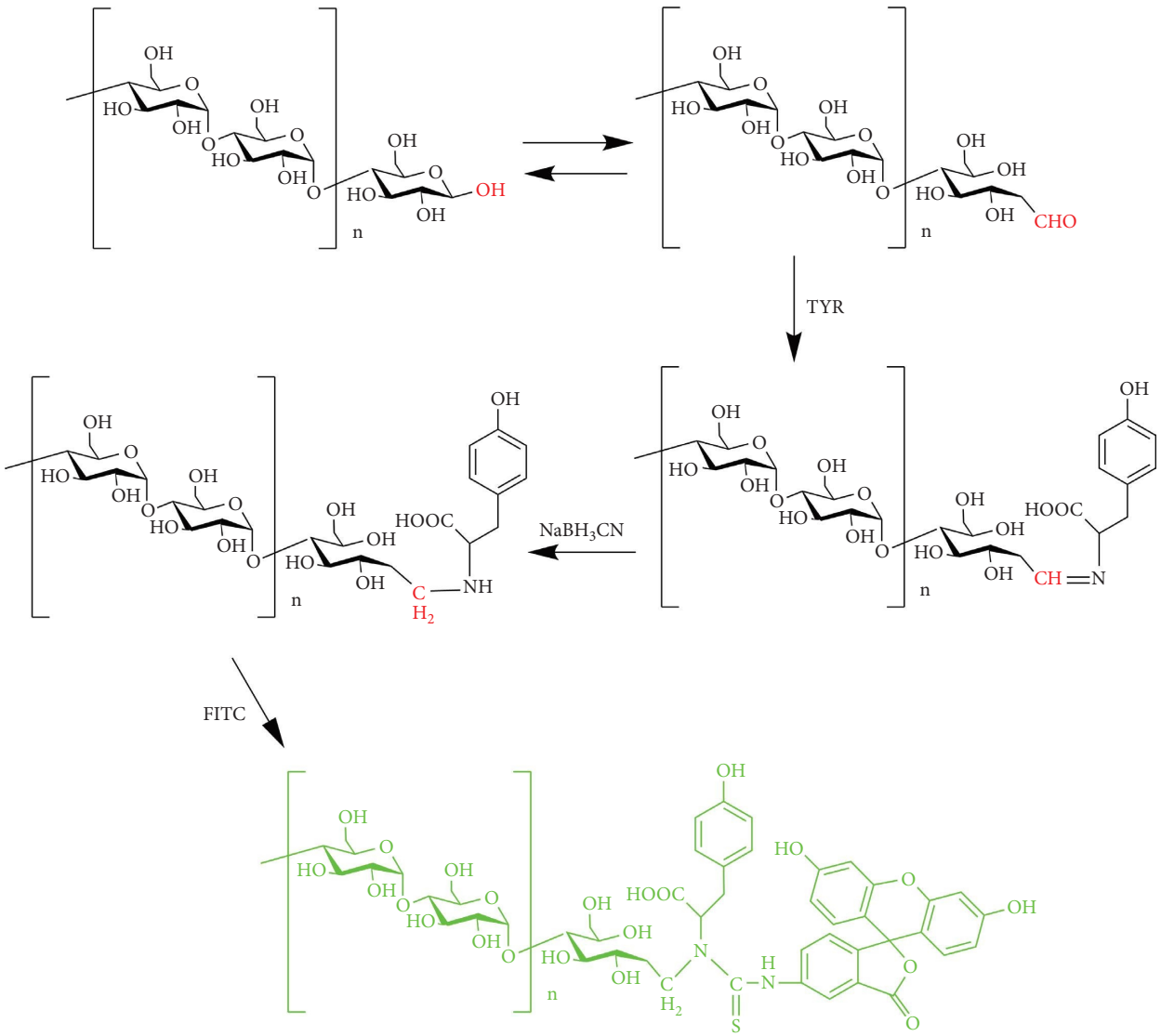

Figure 1: Fluorescence labeling of PLP1-TYR-FITC.

mice. After 14 days of consecutive gavage, we measured serum biochemical indices, such as AST activity, ALT activity, ALP activity, TC level, TG level, and Crea level. Following euthanasia, major organs, including the heart, liver, spleen, lungs, kidneys, brain, colon, and small intestine, were harvested for H&E staining. Briefly, the organs were processed by deparaffinization, rehydration with water, washing, staining, additional washing, drying, and mounting. The results were observed under a light microscope, and images were captured.

2.5.4. In Vivo Imaging Studies of PLP1-TYR-FITC. Following our previous study, the experimental protocol involved administering 100 mg/kg or 50 mg/kg of PLP1-TYR-FITC dissolved in saline [13]. Subsequently, PLP1-TYR-FITC was given to mice via oral gavage and intravenous injection. All animals were randomly assigned to the blank and control groups (under different time nodes, n = six mice/group). Animals in the blank group were given an equivalent amount of saline, whereas those in the control group received 100 mg/kg or 50 mg/kg of PLP1-TYR-FITC via gavage or injection. Considering the FITC substitution rate in PLP1-TYR-FITC, oral administration of 0.53 mg/kg of FITC and intravenous injection of 0.27 mg/kg of FITC were done to prevent FITC interference. Subsequently, mice were anesthetized with 10% bioethanol at 0.5, 1, 2, 4, 5, 6, 12, and 24 h *in vivo* imaging, respectively. The distribution of the fluorescent probe in mice was observed using *in vivo* imaging (IVIS Lumina LT, USA). Finally, plasma and tissue homogenates were collected for quantitative and pharmacokinetic analyses.

2.5.5. Establishing a Method for the Quantification of PLP1-TYR-FITC in Plasma and Tissue Samples

2.5.5.1. Linear Relationship. The methodological experiments followed the study conducted by Dong et al. [15]. Twenty milligrams of PLP1-TYR-FITC was weighed and

diluted to 20 mL by adding PBS to prepare a stock solution (1 mg/mL). The stock solution was kept at 4°C in the dark. Plasma and tissue homogenates from the blank group were prepared by homogenizing plasma and tissues from various organs, such as the brain, small intestine, stomach, kidney, lung, spleen, liver, and heart, with PBS at a 1:9 ratio. Then, the mixtures were centrifuged at 3500 r/min for 10 min to obtain the supernatant. The PLP1-TYR-FITC stock solution was added to plasma and tissue homogenates to prepare specimens with different concentrations (range: 0.1–200 μg/mL). PBS of the same volume was used as a substitute for the PLP1-TYR-FITC solution to detect fluorescence intensities (slit width = 2 nm, E_m = 525 nm, and E_x = 495 nm) of blank plasma and homogenized tissue samples. The fluorescence intensity of plasma and each tissue homogenate was determined as described in Section 2.3, with fluorescence intensity plotted on the y-axis and plasma sample concentration on the x-axis.

2.5.5.2. Precision Test. Two hundred microliters of blank plasma and tissue homogenate were collected. Three different mass concentrations of PLP1-TYR-FITC standard solution, including low concentration (1 μg/mL), medium concentration (10 μg/mL), and high concentration (50 μg/mL), were added to each sample. For blank plasma samples and tissue homogenates, the PLP1-TYR-FITC solution was replaced with an equal volume of PBS. Six samples were prepared for each mass concentration, and each sample was analyzed over 5 days.

2.5.5.3. Stability Test. Three different concentrations of plasma samples and tissue homogenates were prepared using the same method used for the precision solution preparation. Six replicates were prepared for each concentration. Blank plasma and tissue homogenate samples were analyzed using PBS instead of PLP1-TYR-FITC sample solution. The samples were kept at room temperature for 24 h, at 4°C for 14 days, and at 20°C for 15 days.

2.5.5.4. Sample Adding Recovery Test. The procedure was conducted based on the precision solution preparation method. Solutions of plasma and tissue homogenates were prepared with three distinct concentrations (six replicates for each concentration). The recovery of PLP1-TYR-FITC in plasma samples and tissue homogenates was determined by comparing the observed values with the theoretical values.

2.5.6. Pharmacokinetics and Tissue Distribution of PLP1-TYR-FITC. Blood samples were extracted at various time points (0.5, 1, 2, 3, 6, 8, 12, and 24 h) and placed in 1.5-mL brown centrifuge tubes containing heparin. The supernatant was collected as plasma following centrifugation (3500 r/min, 10 min). A 200 μL aliquot of plasma was diluted with PBS to a final volume of 2.5 mL. At the end of the experiment, tissue specimens from the brain, heart, small intestine, stomach, kidney, lung, spleen, and liver were collected. After tissue homogenization, 200 μL of tissue homogenates were diluted to 2.5 mL with PBS. The fluorescence intensities of tissue homogenates were measured using a fluorescence spectrophotometer.

2.6. Statistical Analysis. After a single intravenous injection, the blood concentration data in mice were fitted using the atrial chamber model. Pharmacokinetic parameters were assessed using DAS 2.0 software. All data are presented as mean ± SEM. Data were compared between groups using one-way ANOVA and Tukey's multiple-comparison test. Statistical analyses were conducted using GraphPad Prism 9.0. $p < 0.05$ was considered statistically significant.

3. Results

3.1. Extraction and Purification of PLP1. The crude polysaccharides (PLPs) were obtained through boiling water extraction and alcohol precipitation, yielding 1.75% w.t. Subsequently, PLPs were eluted with deionized water and purified using DEAE-52 cellulose and Sephadex G-75 column anion exchange chromatography column. The polysaccharide composition was assessed using the anthrone–sulfuric acid assay, and then an elution curve was plotted (Figures 2(a) and 2(b)). Based on the elution curves, the fraction with the highest concentration of polysaccharides was collected and designated as PLP1. Additionally, the total sugar content in PLP1 was determined to be 94.72%, suggesting that PLP1 is a neutral polysaccharide [1].

3.2. Marking of PLP1-TYR-FITC. The UV–vis scanning spectra of PLP1, PLP1-TYR, and PLP1-TYR-FITC were compared, indicating the significant absorption peaks of PLP1-TYR-FITC near 280 and 495 nm and suggesting the successful binding of FITC after amination (Figures 3(a), 3(b), and 3(c)). The absorption peak at around 230 nm is likely attributed to the π to $\pi*$ electronic transitions associated with the aromatic rings present in TYR and FITC. Furthermore, the IR spectrum of PLP1-TYR-FITC showed characteristic bands for O–H (3415.99 cm^{-1}), C–H (2927.88 cm^{-1}), C–N (2170 cm^{-1}), and C=S (1341 cm^{-1}), suggesting the successful addition of fluorophores to PLP1 molecules (Figure 3(d)).

Moreover, a comparison of the ^{1}H NMR spectrum of PLP1-TYR-FITC with those of PLP1 and FITC revealed characteristic signals of double bonds originating from FITC in the PLP1-TYR-FITC conjugate, confirming successful synthesis (Figure 4).

In the HPGPC chromatogram, PLP1 and PLP1-TYR--FITC revealed a single symmetrical peak, with only the peak time-shifted. The purity of both PLP1 and PLP1-TYR-FITC was more than 98.0% (Figures 5(a) and 5(b)). The results obtained from PLP1, FITC, and PLP1-TYR-FITC samples using the Duetta-Horiba Fluorescence and Absorbance spectrometer also confirmed the introduction of the fluorescent moiety (Figure 5(c)).

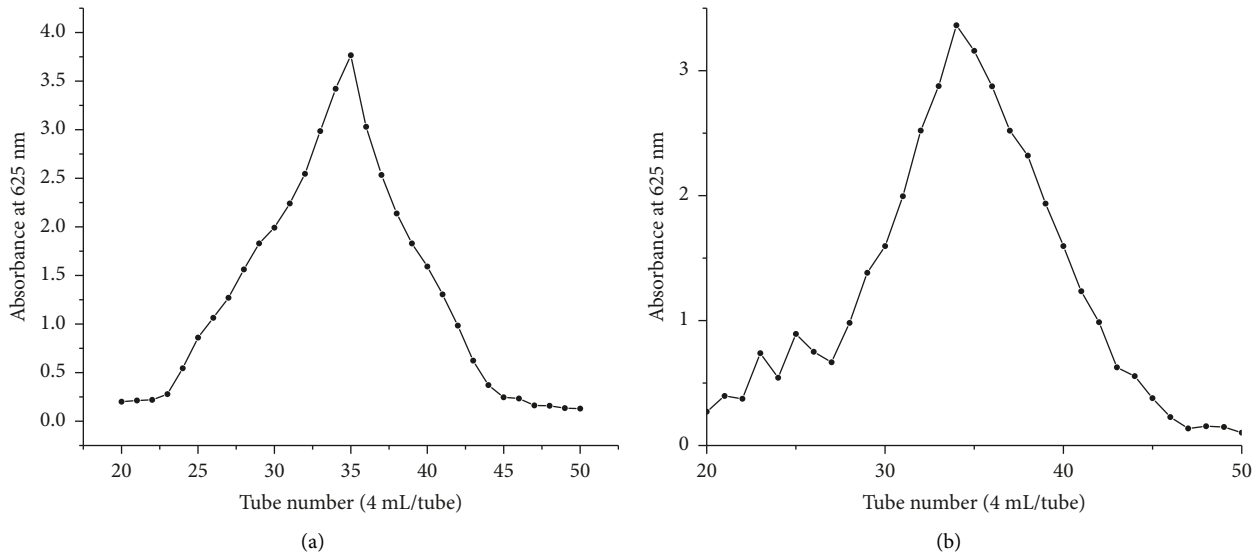

Figure 2: (a) DEAE-52 elution curves. (b) Sephadex G-75 elution curve analysis.

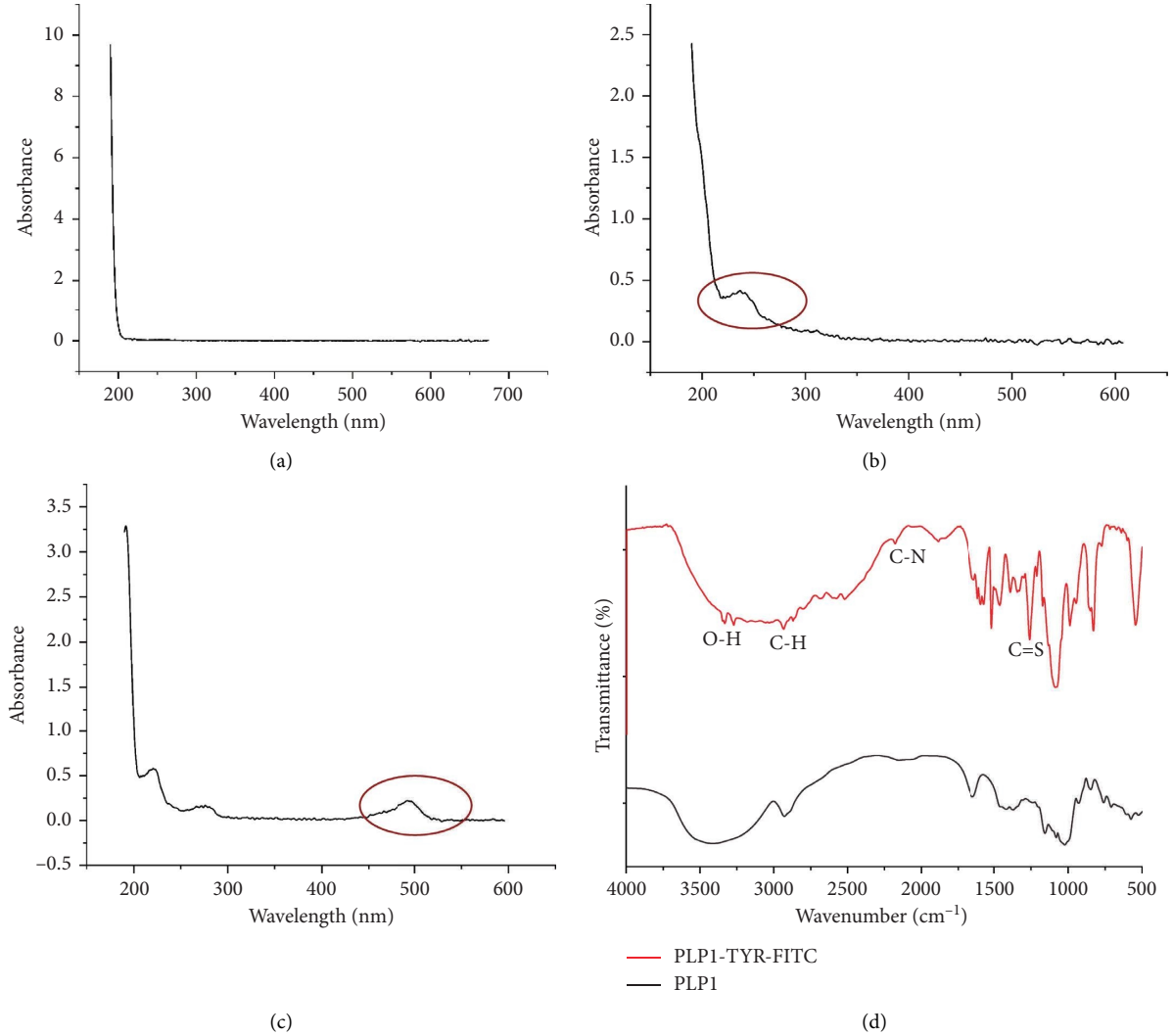

Figure 3: (a) UV characteristics of PLP1, (b) PLP1-TYR, (c) PLP1-TYR-FITC, and (d) FT-IR spectra of PLP1-TYR-FITC and PLP1.

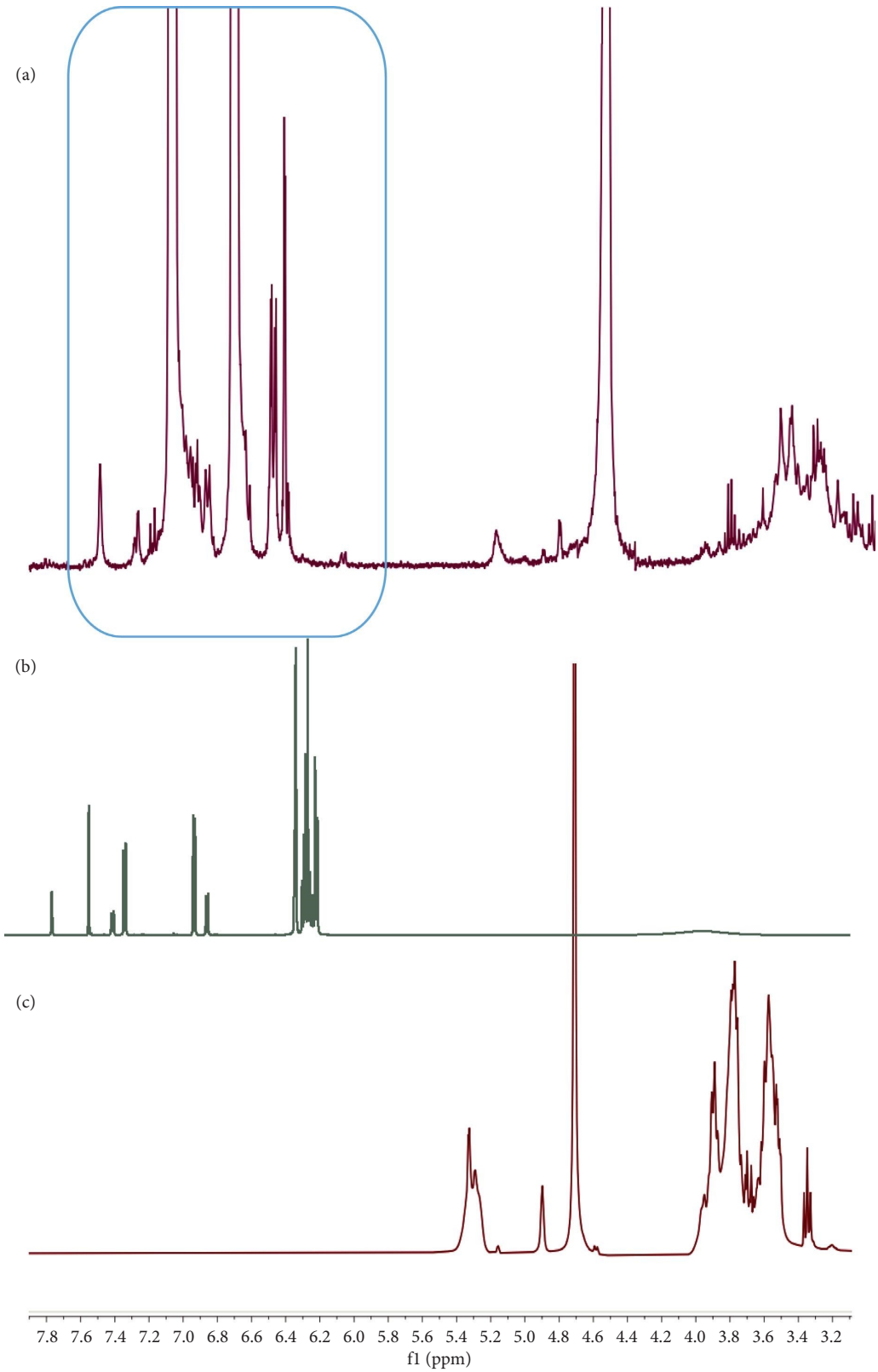

Figure 4: ^{1}H spectra of (a) PLP1-TYR-FITC, (b) FITC, and (c) PLP1.

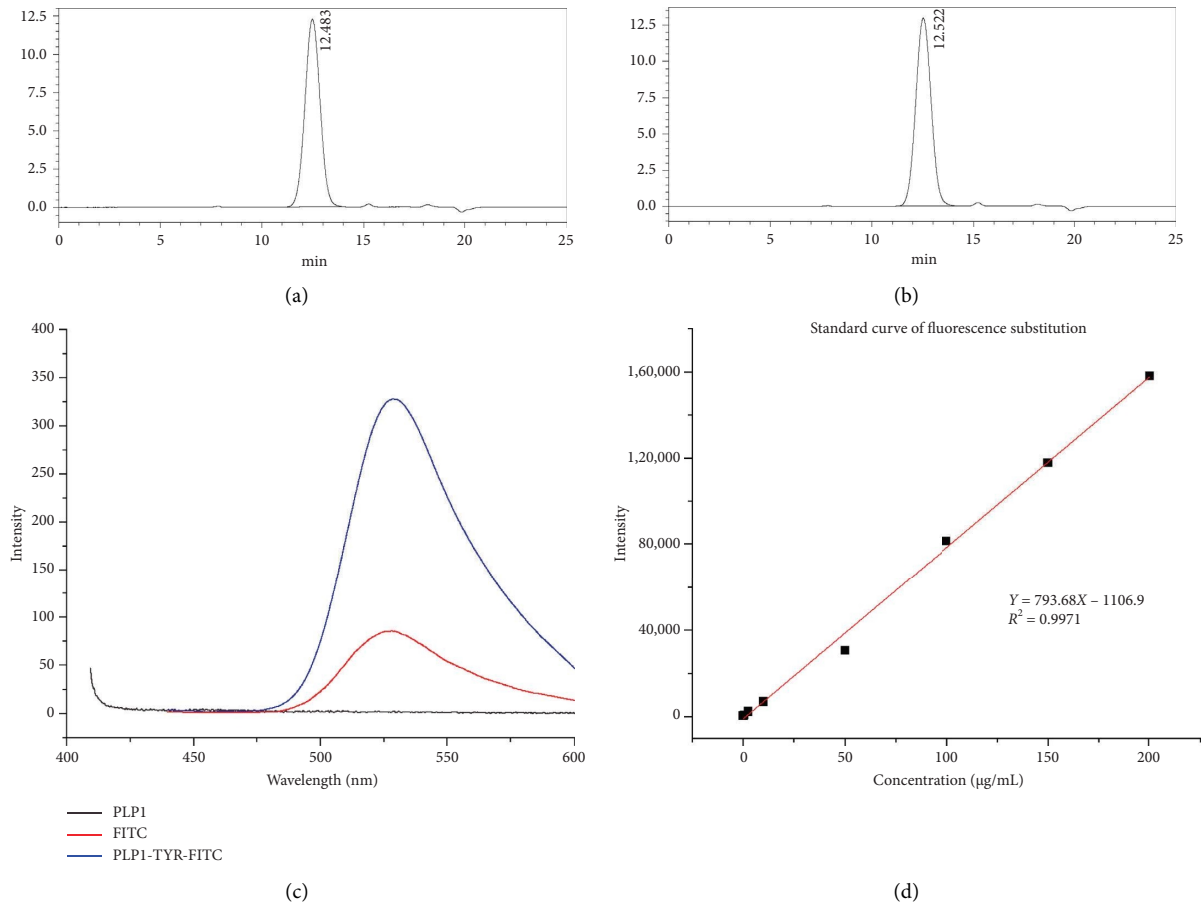

Figure 5: (a) HPGPC of PLP1, (b) PLP1-TYR-FITC, (c) fluorescence intensities of PLP1, FITC, and PLP1-TYR-FITC, and (d) standard curve for fluorescence substitution.

3.3. Analysis of Fluorescence Substitution Levels. The standard curve for PLP1-TYR-FITC was drawn using the following equation: $Y = 793.68X - 1106.9$, with an R^2 value of 0.9971 (Figure 5(d)). Using this equation, the fluorescence substitution level was determined to be 0.53%, suggesting that 100 μg of PLP1-TYR-FITC consisted of 0.53 μg FITC after labeling with fluorescence.

3.4. The Results of Fluorescence Microscopy. The results of MTT indicated that PLP1-TYR-FITC exerted no cytotoxic effects on HepG2 cells and AML12 cells within the range of 100–1600 μg/mL (Figures 6(a) and 6(b)). Fluorescence micrographs of HepG2 and AML12 cells are shown in Figures 6(c) and 6(d). Compared to cell lines incubated with PLP1-TYR-FITC alone, no significant fluorescence was observed in either cell line after treatment with the intracellular endocytosis inhibitor. These results suggest that PLP1-TYR--FITC may enter the cells by endocytosis, providing direct evidence for its physiological activity at the cellular level.

3.5. Acute Toxicity Test. During the entire experimental period, mice in the polysaccharide fluorescent probe test group receiving 2000 mg/kg of polysaccharide fluorescent probe via gavage exhibited no signs of toxicity or mortality. Their mental state and behavior remained normal and comparable to those in the normal group. Additionally, their feces exhibited normal color and consistency, their fur appeared smooth and glossy, and they achieved normal body weight gain. These observations suggest that PLP1-TYR--FITC is nontoxic and poses no harmful effects.

3.6. Subacute Toxicity Test. A subacute toxicity test was conducted on mice to assess the safety of PLP1-TYR-FITC, and the serological indexes were detected (Table 1). The serological indexes of mice treated with PLP1-TYR-FITC gavage did not reveal marked abnormalities compared to those of the normal group.

Meanwhile, the main tissues of mice were collected for H&E staining of the heart, liver, spleen, lungs, kidneys, brain, small intestines, and colon. H&E staining indicated that all tissues were similar to the normal group. The results indicated that PLP1-TYR-FITC is a safe and nontoxic active ingredient and can be used for subsequent studies.

3.7. Validated Method for Quantifying PLP1-TYR-FITC in Plasma and Tissue Samples

3.7.1. Linear Relationship. The standard curve was generated using the concentrations of PLP1-TYR-FITC as the abscissa (X) and the fluorescence intensities as the ordinate (Y). The

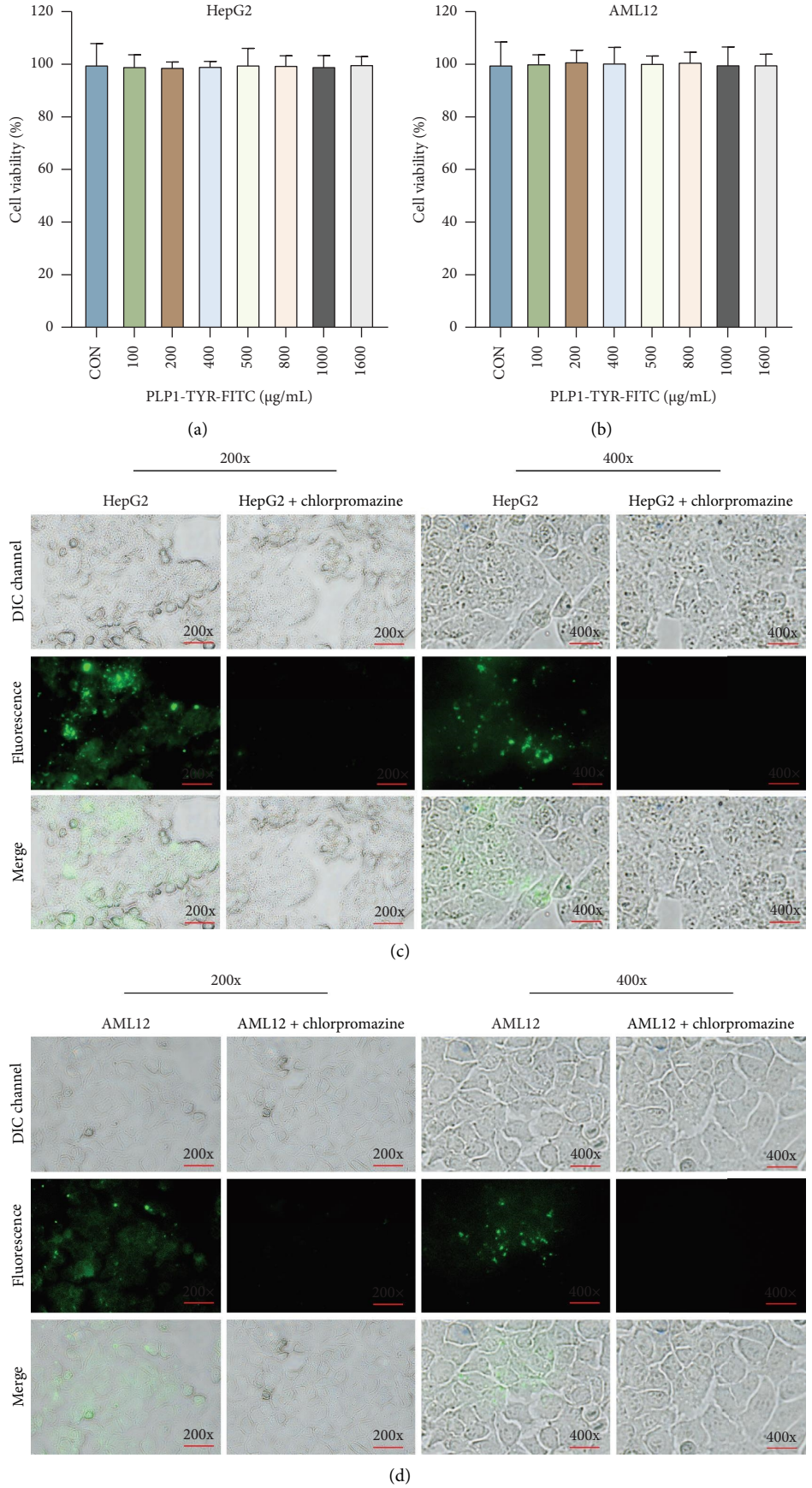

Figure 6: (a) MTT result of HepG2 cells, (b) MTT result of AML12 cells, (c) HepG2 cells (with inhibitor added) were incubated with PLP1-TYR-FITC, and (d) AML12 cells (with inhibitor added) were incubated with PLP1-TYR-FITC.

Table 1: The results of the subacute toxicity test of PLP1-TYR-FITC.

Index	Normal group	1000 mg/kg	2000 mg/kg
ALT (U/L)	32.71 ± 1.14	31.95 ± 1.22	32.86 ± 1.56
AST (U/L)	38.49 ± 1.08	39.3 ± 1.73	36.71 ± 1.25
ALP (U/L)	51.36 ± 2.01	50.47 ± 1.96	52.14 ± 1.38
TC (mmol/L)	3.11 ± 0.25	3.09 ± 0.17	3.27 ± 0.44
TG (mmol/L)	1.82 ± 0.37	1.85 ± 0.41	1.79 ± 0.35
Crea (μmol/L)	45.4 ± 1.28	46.22 ± 1.49	44.93 ± 1.42

R^2 values in plasma and tissue specimens ranged from 0.9924 to 0.9987, indicating a robust linear relationship in the range of 0.1–200 μg/mL. The correlation coefficient, regression equation, and linear range are summarized in Table 2, all conforming to the criteria for linear dynamics.

3.7.2. Precision Test. Table 3 presents the intraday and interday precision of PLP1-TYR-FITC in plasma and tissue specimens. The results demonstrated that the method possesses high precision, with matrix effects in plasma and tissue specimens being negligible, thus ensuring accurate determination of the drug concentrations *in vivo*. The relative error percentage (RE%) was calculated using the following formula:

$$\mathrm{RE\%} = \left(\frac{\text{Measured Value} - \text{True Value}}{\text{True Value}}\right) \times 100. \quad (1)$$

3.7.3. Stability Test. Table 4 presents the results of the stability experiments. The stability of PLP1-TYR-FITC was assessed under three conditions: room temperature, refrigeration at 4°C, and freezing at −20°C. Thereafter, the results of different conditions were compared. PLP1-TYR-FITC demonstrated good stability across all conditions.

3.7.4. Sample Adding Recovery Test. Table 5 presents the recovery of PLP1-TYR-FITC spiked into plasma and tissue specimens. PLP1-TYR-FITC exhibited good recovery in both plasma and tissue specimens.

Based on the results of linearity, precision, stability, and recovery tests, we successfully constructed a method for measuring PLP1-TYR-FITC in plasma and tissue samples.

3.8. Concentration–Time Profiles, Pharmacokinetic Parameters, and Distribution in Different Tissues of PLP1-TYR-FITC in Mice. After oral administration and intravenous injection, the concentrations of PLP1-TYR-FITC (100 or 50 mg/kg) were measured at 0.5–24 h. The concentrations were plotted against the corresponding time points to generate a concentration–time profile (Figure 7). Notably, the highest blood concentration of PLP1-TYR-FITC was measured at 0.5 h after a single intravenous injection. Thereafter, a gradual decrease was observed with time, accompanied by a slowing rate. Meanwhile, after a single dose

Table 2: Standard curves of PLP1-TYR-FITC in plasma and tissue samples.

Tissue	Linear equation	Linearity range (μg/mL)	R^2
Plasma	$y = 2.2170x + 60.734$	0.1–200	0.9961
Heart	$y = 1.6735x + 79.818$	0.1–200	0.9984
Liver	$y = 1.7004x + 184.140$	0.1–200	0.9954
Spleen	$y = 2.3869x - 7.797$	0.1–200	0.9983
Lung	$y = 2.6613x + 29.759$	0.1–200	0.9958
Kidney	$y = 2.3020x + 77.277$	0.1–200	0.9961
Stomach	$y = 1.7852x + 27.874$	0.1–200	0.9956
Small intestine	$y = 1.4176x + 64.495$	0.1–200	0.9984
Brain	$y = 2.3195x - 30.870$	0.1–200	0.9920

of gavage, the plasma concentration of PLP1-TYR-FITC increased most rapidly within 0.5–1 h and then decreased slowly with time.

Pharmacokinetic parameters were calculated and compared using DAS 2.0 software. The results are presented in Table 6. We calculated the actual administered dose of FITC (0.27 mg/kg) based on the substitution rate (0.53%) and determined the pharmacokinetic parameters of FITC to indicate that the metabolism of FITC does not significantly affect the original metabolic pathways of PLP1-TYR-FITC. The results indicated that the pharmacokinetic characteristics of PLP1-TYR-FITC are significantly different from those of free FITC (Table S1). The main calculated parameters were area under the curve (AUC), maximum concentration (C_{max}), and half-life period ($t_{1/2\alpha}$).

After 8 h of intragastric administration and intravenous injection, fluorescence intensity was measured after autopsy and homogenization of major organs. The results are depicted in Figure 8. After gavage and intravenous administration, PLP1-TYR-FITC was mainly concentrated in the liver, kidney, and small intestine.

3.9. In Vivo Imaging Experiments. Real-time fluorescence imaging was conducted after gavage (Figure S1A). Fluorescence was primarily observed in the stomach and small intestine within the initial 6 h, indicating the absorption process of PLP1 *in vivo* (Figures S1B and S1C). After 8 h, strong fluorescence intensity was detected in the small intestine and liver, indicating the metabolism of PLP1 in these organs and suggesting the preferential enrichment of PLP1 in the liver. Only the small intestine showed weak fluorescence after 12 h (Figure S1D).

Table 3: Intraday and interday precisions of PLP1-TYR-FITC in plasma and tissue specimens.

Tissue	Conc (μg/mL)	Found conc (μg/mL)	Accuracy (RE%)	Interday RSD (%)	Intraday RSD (%)
Plasma	1	1.01 ± 0.11	1.92	0.55	3.98
	10	12.42 ± 0.37	−7.98	1.47	6.55
	50	50.26 ± 0.62	9.02	2.38	6.07
Heart	1	0.98 ± 0.15	−2.55	13.28	4.62
	10	11.3 ± 0.24	−2.9	17.56	9.64
	50	50.79 ± 0.96	3.11	15.83	8.53
Liver	1	0.99 ± 0.18	−3.34	17.35	18.13
	10	12.43 ± 0.15	−3.78	16.49	14.54
	50	50.74 ± 0.52	−4.13	18.38	17.62
Spleen	1	1.01 ± 0.39	−1.75	9.07	14.9
	10	10.68 ± 0.34	−6.56	15.48	10.87
	50	50.36 ± 0.77	−1.04	10.06	8.02
Lung	1	1.07 ± 0.2	−6.28	10.65	7.1
	10	10.75 ± 0.31	−2.16	17.02	7.99
	50	50.29 ± 1.04	−8.57	18.34	18.64
Kidney	1	0.98 ± 0.27	2.07	14.12	7.25
	10	10.05 ± 0.38	1.62	17.57	13.19
	50	49.96 ± 0.93	−1.08	16.3	7.84
Stomach	1	0.97 ± 0.16	−3.67	9.24	3.56
	10	10.07 ± 0.58	−7.05	7.58	1.44
	50	51.02 ± 0.33	−2.17	8.73	6.02
Small intestine	1	0.99 ± 0.08	−3.25	12.24	5.61
	10	11.02 ± 0.67	4.19	10.16	12.17
	50	50.01 ± 0.24	−9.85	13.73	4.26
Brain	1	1.07 ± 0.22	−9.6	14.33	5.12
	10	10.28 ± 0.41	9.58	13.09	4.95
	50	49.7 ± 0.86	−3.52	12.77	5.17

Table 4: The stability of PLP1-TYR-FITC in plasma and tissue specimens.

Tissue	Conc (μg/mL)	RT for 24 h		−4°C for 14 days		−20°C for 15 days	
		Found conc (μg/mL)	RSD (%)	Found conc (μg/mL)	RSD (%)	Found conc (μg/mL)	RSD (%)
Plasma	1	1.33 ± 0.14	7.65	1.02 ± 0.16	8.24	0.97 ± 0.08	5.17
	10	10.05 ± 0.28	5.26	9.65 ± 0.56	6.39	10.02 ± 0.13	4.52
	50	51.07 ± 0.76	10.07	50.24 ± 0.85	7.32	49.67 ± 0.69	6.57
Heart	1	0.95 ± 0.08	6.02	1.13 ± 0.28	10.83	1.04 ± 0.35	8.23
	10	9.72 ± 0.64	5.1	10.16 ± 0.51	13.27	9.85 ± 0.21	7.69
	50	48.69 ± 0.58	12.87	50.04 ± 0.63	11.59	49.66 ± 0.74	5.64
Liver	1	0.92 ± 0.15	4.76	0.89 ± 0.06	5.54	1.07 ± 0.39	6.27
	10	9.26 ± 0.41	7.98	9.53 ± 0.17	8.91	10.01 ± 0.34	7.92
	50	51.38 ± 0.96	5.25	50.65 ± 0.44	8.1	49.89 ± 0.82	8.63
Spleen	1	1.07 ± 0.09	6.67	1.22 ± 0.09	6.73	1.05 ± 0.1	10.28
	10	10.39 ± 0.88	9.85	9.82 ± 0.68	10.02	10.04 ± 0.35	11.44
	50	50.26 ± 0.95	5.62	51.58 ± 0.86	7.35	50.24 ± 0.84	13.68
Lung	1	1.08 ± 0.34	10.1	1.05 ± 0.12	11.26	1.13 ± 0.24	7.56
	10	9.97 ± 0.51	12.54	9.64 ± 0.71	10.68	10.25 ± 0.16	14.21
	50	48.95 ± 1.02	11.06	49.65 ± 0.91	13.17	50.06 ± 0.93	13.14
Kidney	1	1.02 ± 0.17	6.93	1.53 ± 0.35	8.98	1.38 ± 0.27	9.74
	10	10.38 ± 0.81	7.55	11.05 ± 0.41	8.13	10.6 ± 0.22	10.58
	50	50.05 ± 1.2	10.18	51.12 ± 0.9	5.6	49.97 ± 1.05	13.16
Stomach	1	1.21 ± 0.09	12.04	1.16 ± 0.18	10.37	1.4 ± 0.08	6.56
	10	10.16 ± 0.32	10.88	9.97 ± 0.1	11.62	10.19 ± 0.34	8.11
	50	49.76 ± 0.8	11.26	50.46 ± 0.57	10.54	50.06 ± 0.59	9.14

Table 4: Continued.

Tissue	Conc (μg/mL)	RT for 24 h		−4°C for 14 days		−20°C for 15 days	
		Found conc (μg/mL)	RSD (%)	Found conc (μg/mL)	RSD (%)	Found conc (μg/mL)	RSD (%)
Small intestine	1	1.32 ± 0.56	9.66	1.54 ± 0.17	10.04	1.44 ± 0.32	8.53
	10	13.06 ± 0.72	11.34	12.15 ± 0.88	6.71	12.76 ± 0.91	13.21
	50	51.68 ± 1.01	10.68	49.44 ± 0.56	13.24	50.15 ± 0.62	11.29
Brain	1	0.96 ± 0.07	11.39	1.03 ± 0.09	11.9	1.15 ± 0.64	8.5
	10	10.15 ± 0.57	7.24	9.36 ± 0.37	9.65	9.14 ± 0.36	7.44
	50	50.64 ± 0.84	5.42	50.98 ± 0.75	10.44	50.02 ± 0.55	6.17

Table 5: Sample recovery rate of PLP1-TYR-FITC in plasma and tissue specimens.

Tissue	Conc (μg/mL)	Found conc (μg/mL)	Recovery (%)	RSD (%)
Plasma	1	0.92 ± 0.07	98.33	4.82
	10	10.08 ± 0.39	97.42	5.16
	50	50.86 ± 0.81	102.61	1.74
Heart	1	1.03 ± 0.14	104.74	8.62
	10	11.31 ± 0.29	102.73	2.07
	50	49.45 ± 0.62	98.2	1.36
Liver	1	1.14 ± 0.23	99.14	2.54
	10	9.82 ± 0.16	105.55	10.48
	50	51.22 ± 0.93	100.74	9.53
Spleen	1	0.95 ± 0.09	99.52	4.27
	10	10.36 ± 0.23	101.98	3.27
	50	50.74 ± 0.57	100.78	2.63
Lung	1	1.1 ± 0.26	99.93	1.34
	10	10.75 ± 0.34	101.62	5.48
	50	50.01 ± 1.15	99.31	4.98
Kidney	1	1.02 ± 0.3	103.77	11.3
	10	10.51 ± 0.22	100.23	1.32
	50	50.26 ± 0.86	100.45	10.93
Stomach	1	0.97 ± 0.18	99.03	4.05
	10	9.88 ± 0.15	103.26	7.54
	50	49.89 ± 0.72	103.31	8.52
Small intestine	1	1.16 ± 0.27	101.79	6.81
	10	11.07 ± 0.41	99.76	2.89
	50	51.46 ± 1.05	102.53	11.27
Brain	1	0.94 ± 0.08	99.86	9.49
	10	10.49 ± 0.25	104.25	7.6
	50	50.73 ± 0.84	100.46	5.77

Meanwhile, real-time fluorescence imaging was also conducted after intravenous administration (Figure S2A). Fluorescence was mainly concentrated in the liver, kidneys, and small intestine (Figures S2B and S2D). After 8 h, the strongest fluorescence intensity was detected in the liver. These results are consistent with the hepatoprotective properties of PLP1 reported in our previous study [1]. After 24 h of administration, green fluorescence was detected in mice urine, albeit with reduced intensity, confirming drug excretion.

Overall, the *in vivo* fluorescence tracer results of PLP1-TYR-FITC effectively delineated the metabolic pathway of PLP1 absorption. It was absorbed in the small intestine, metabolized in the liver and kidneys, and finally excreted primarily through urine. To the best of our knowledge, this is the first study reporting the metabolic pathway of *Pueraria* polysaccharide *in vivo*, providing a foundation for the development and utilization of PLP1 as a novel *Pueraria* polysaccharide and paving the way for further studies into its mechanisms of action.

4. Discussion

In this study, the amination reduction approach was applied to label the reducing end of *P. lobata* polysaccharides, resulting in the formation of PLP1. In addition, PLP1 was selectively tagged with the fluorescent marker FITC for the first time. Thorough experiments were conducted to comprehensively characterize the fluorescent probe PLP1-TYR-FITC derived from *P. lobata*. *In vitro,* fluorescence microscopy demonstrated that PLP1-TYR-FITC may enter the cells by endocytosis. Pharmacokinetic and *in vivo*

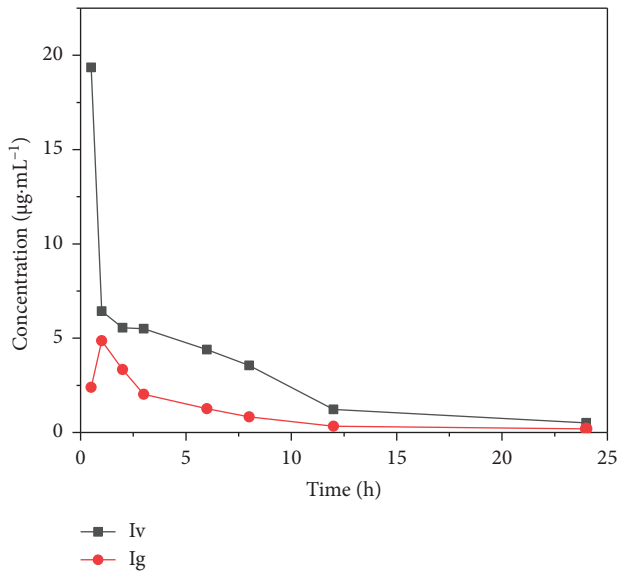

Figure 7: Concentration–time profile of PLP1-TYR-FITC in mice after oral administration and intravenous injection.

Table 6: Pharmacokinetic parameters of PLP1-TYR-FITC in mice after single intragastric administration and intravenous injection.

Pharmacokinetic parameters	I.g. (100 mg/kg)	I.v. (50 mg/kg)
AUC (0-t) (mg/L∗h)	14.125	60.363
AUC (0-∞) (mg/L∗h)	15.389	68.13
Cm_{ax} (mg/L)	4.862	19.350
$t_{1/2\alpha}$ (h)	69.315	0.05

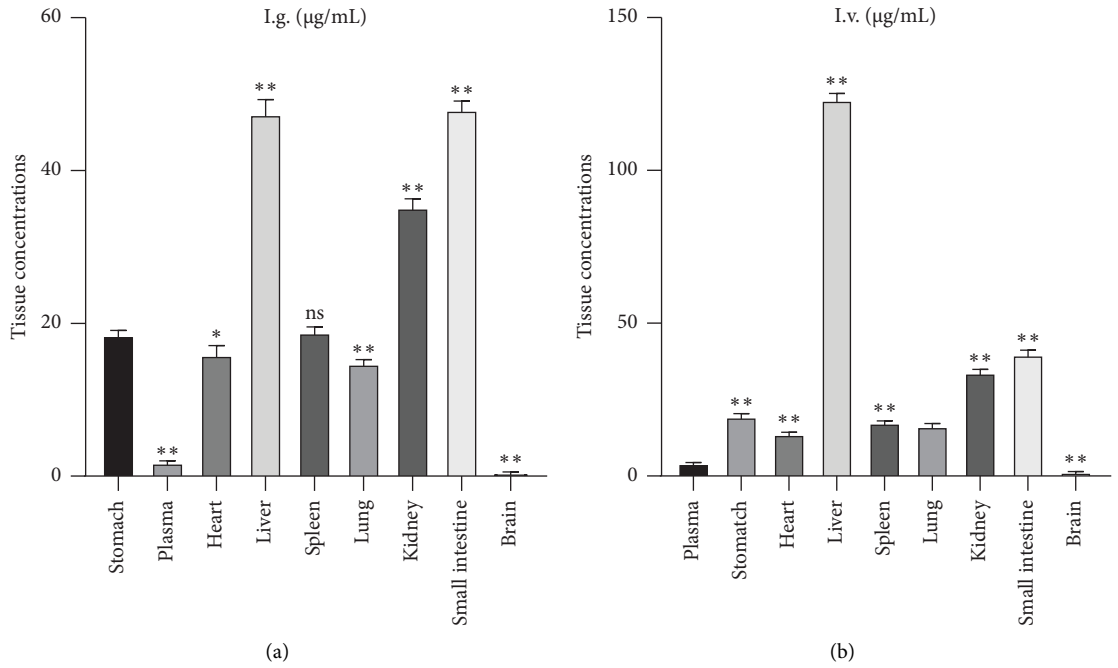

Figure 8: The tissue concentrations of PLP1-TYR-FITC in mice 8 h after single intragastric administration and intravenous injection. $^{*}p < 0.05$, $^{**}p < 0.01$ versus stomach or plasma.

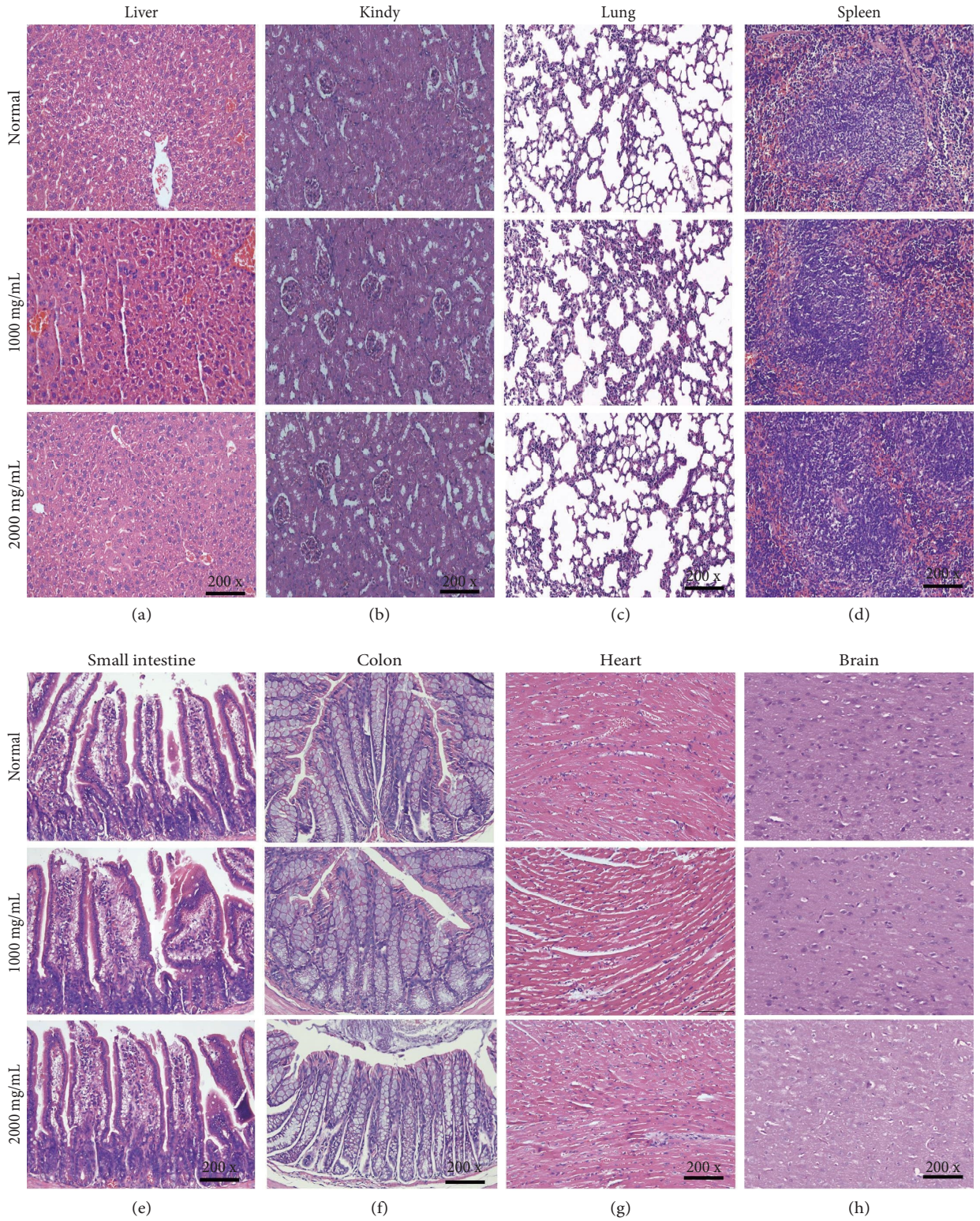

Figure 9: H&E staining of (a) the liver, (b) kidney, (c) lung, (d) spleen, (e) small intestine, (f) colon, (g) heart, and (h) brain.

imaging revealed that the fluorescent probe-labeled PLP1 was predominantly localized in liver tissues.

For centuries, polysaccharides have served as natural resources for supplements and medicines to treat various diseases. However, their complex structures, large molecular weights, and lack of luminescent properties made their *in vitro* mechanistic assessment and *in vivo* pharmacokinetics studies challenging. There is no direct and effective evidence on whether these biomacromolecules can bind to cells *in vitro* and target organs *in vivo*. Recently, researchers

have sought to overcome these limitations by considering the fact that most polysaccharides have reduced termini. They have attempted to chemically conjugate fluorescent substances to sugar chains to visualize polysaccharides. For instance, the combination of carboxymethyl chitosan with FITC has been studied in rats undergoing gavage, with the highest levels of carboxymethyl (CM) chitosan detected in the liver [16]. Additionally, a method was established based on HPGPC-FD to specifically and sensitively detect FITC-ROP in rat plasma and tissues (spleen, liver, heart, lungs, kidneys, stomach, and brain). The method targeted fructans extracted from *Radix Ophiopogonis* (ROP) with a mean molecular weight of 4.8 kDa [17]. Similarly, N-galactosylated chitosan (GC) polymers were targeted in the liver using FITC [18]. However, studies on the synthesis of fluorescent probes for *Pueraria lobata* polysaccharides and related pharmacokinetic studies remain limited.

Various fluorescent substances, such as 8-aminonaphthalin-1, 3,6-sulfonic acid (ANTS), 6-aminoquinoline (AQ), 2-aminopyridine (AP), and 4-aminobenzyl cyanide (ABN), can covalently bind to polysaccharides. It is crucial to ensure that the labeled polysaccharide retains the original structure of the natural polysaccharide to accurately track its behavior *in vivo*. However, labeling polysaccharides may alter their pharmacokinetic characteristics by modulating their physicochemical properties, such as molecular weight [18], charge [19, 20], and monosaccharide composition [21]. The results can be affected by polysaccharide dosage [22] and physiological state [23, 24]. Strict control of the substitution degree of polysaccharide labels (< 2.5%) is necessary to mitigate the effect of polysaccharide labeling on their basic structure [12].

PLP1, isolated from *Pueraria lobata*, is a typical water-soluble glucan. The terminal hydroxyl group of C-5 of the main glycosidic unit forms a hemiacetal structure with the aldehyde group of C-1 in its structure, thereby reacting with primary amino groups to form Schiff bases [21, 25]. Due to the reversible nature of this reaction, there is an equilibrium between open and closed loops in solution, resulting in a certain proportion of reduced aldehyde groups. Sodium cyanoborohydride specifically reduces the double bond within the Schiff base without affecting the aldehyde group, irreversibly shifting the reaction toward the product. However, this reduction process is slow and needs sufficient time. By adding tyramine, the amino group binds to the semi-aldehyde group of polysaccharides. Subsequently, the introduced amino group covalently binds to FITC's isothiocyanate in an alkaline environment (Figure 1) [26, 27]. The FITC used in this experiment had low molecular weight, and the polysaccharide had few reduction ends. The labeling efficiency of the polysaccharide was 0.53%, markedly less than the 2.5% threshold. Therefore, the activity of PLP1 did not significantly change after labeling.

In this study, FITC was incorporated into the terminus of PLP1. The findings demonstrated that polysaccharides had no characteristic peaks at 260 and 280 nm, suggesting the removal of free nucleic acids and proteins. On the contrary, FITC displayed a characteristic peak at 495 nm. During PLP1-TYR-FITC synthesis, peaks appeared simultaneously at 280 and 495 nm, confirming that PLP1 was covalently bound to FITC after adding amine groups (Figures 3(a), 3(b), and 3(c)). PLP1-TYR-FITC was also characterized through integrated analysis combining fluorescence and high-performance gel permeation chromatography, as well as Fourier infrared, ultraviolet, and nuclear magnetic resonance analyses. The calculated fluorescence substitution rate was 0.53%, suggesting that PLP1 can bind to the fluorescent probe. Additionally, the distribution and pharmacokinetic characteristics of PLP1 labeled with fluorescent probes were investigated *in vitro* and *in vivo*. The results unequivocally revealed that PLP1-TYR-FITC entered the cells through endocytosis when incubated with HepG2 cells and AML12 cells under photoprotection for 2 h. These findings support the hepatoprotective properties of PLP1 at the cellular level (Figure 6). Toxicity assessments demonstrated that PLP1-TYR-FITC is safe and nontoxic (Figure 9 and Table 1). After establishing methodological prerequisites for in vivo administration via gavage and intravenous injection, it was observed that the PLP1-TYR-FITC was mainly absorbed and metabolized in the small intestine, liver, and kidneys (Figure 7, Tables 2, 3, 4, and 5). In real-time fluorescence imaging, fluorescence mainly appeared in the small intestine of mice within the first 6 h, indicating that the absorption process of PLP1 *in vivo* primarily occurred through the small intestine in the initial 6 h after oral administration and intravenous injection. After 8–12 h, PLP1 was metabolized in the liver and kidney, evidenced by the strongest fluorescence intensity in these organs. These findings suggest that PLP1 can accumulate in the liver and exert its hepatoprotective effects. Finally, only faint green fluorescence was detected in urine, confirming that PLP1 was primarily excreted in urine (Figures S1 and S2).

5. Conclusions

We successfully labeled the reducing end of PLP1 with the selective fluorescent marker FITC using the amination reduction method, as the first application of this technique for PLP1. The characterization of PLP1-TYR-FITC was conducted through a comprehensive analysis of spectroscopic data. Fluorescence microscopy indicated that PLP1-TYR-FITC may enter the cells by endocytosis. Meanwhile, toxicity assessments revealed that PLP1-TYR-FITC was safe and nontoxic both *in vitro* and *in vivo*. Furthermore, we successfully developed a method to quantitatively measure PLP1-TYR-FITC in plasma and tissues. PLP1-TYR-FITC can be distributed in tissues by two methods of administration. It primarily exists in the small intestine, is absorbed by the liver, and is finally eliminated from the body. These findings provide direct evidence for the physiological function of PLP1 *in vivo* and *in vitro*, laying a theoretical foundation for the development of PLP1 from *Radix Pueraria lobata* as a hepatoprotective agent.

Data Availability Statement

Data are available on request from the authors.

Conflicts of Interest

The authors declare no conflicts of interest.

Author Contributions

Wen Cao: project administration and writing–original draft; Qiuyue Lv: methodology and validation; Xin Zhan: formal analysis and validation; Shihan He: investigation; Jie Yu: validation; Zhu Yang: validation; Guodong Wang: data curation and visualization; Jiangping Wu: data curation, writing–review, and editing; Jun Han: funding acquisition, resources, and supervision. All authors read and approved the final manuscript. Wen Cao and Qiuyue Lv contributed equally to this work.

Funding

This work was supported by the Academic Support Project for Top-Notch Talents in Disciplines of Universities in Anhui Province (gxbjZD2022043), the Project of Natural Science Foundation of the Department of Education of Anhui Province (2024AH040169, 2024AH051934, and 2024AH051923), the Research Funds of Center for Xin'an Medicine and Modernization of Traditional Chinese Medicine of IHM (2023CXMMTCM011), the Inheritance and Innovation Research of TCM of Anhui Province (2024CCCX260 and 2024CCCX016), and the Open Fund of High-level Key Discipline of Chemistry of Chinese Medicine of the State Administration of Traditional Chinese Medicine, Anhui University of Chinese Medicine (HKDCCM2024008).

Supporting Information

Additional supporting information can be found online in the Supporting Information section. *(Supporting Information)*

Supporting file: Pharmacokinetic parameters of FITC in mice after single intragastric administration and intravenous injection and fluorescence imaging of mice at different time points (intravenous injection).

References

[1] W. Cao, J. Wu, X. Zhao, et al., "Structural Elucidation of an Active Polysaccharide From Radix Puerariae lobatae and its Protection Against Acute Alcoholic Liver Disease," *Carbohydrate Polymers* 325 (2024): 121565.

[2] J. Wang, G. Dai, M. Shang, et al., "Extraction, Structural-Activity Relationships, Bioactivities, and Application Prospects of *Pueraria lobata* Polysaccharides as Ingredients for Functional Products: A Review," *International Journal of Biological Macromolecules* 243 (2023): 125210.

[3] Y. Rao, Q. Wen, R. Liu, et al., "PL-S2, a Homogeneous Polysaccharide From Radix Puerariae lobatae, Attenuates Hyperlipidemia via Farnesoid X Receptor (FXR) Pathway-Modulated Bile Acid Metabolism," *International Journal of Biological Macromolecules* 165 (2020): 1694–1705.

[4] G. Cai, C. Wu, T. Zhu, et al., "Structure of a *Pueraria root* Polysaccharide and its Immunoregulatory Activity on T and B Lymphocytes, Macrophages, and Immunosuppressive Mice," *International Journal of Biological Macromolecules* 230 (2023): 123386.

[5] Y. Li, M. Dai, L. Wang, and G. Wang, "Polysaccharides and Glycosides From *Aralia echinocaulis* Protect Rats From Arthritis by Modulating the Gut Microbiota Composition," *Journal of Ethnopharmacology* 269 (2021): 113749.

[6] M. Ding, Z. Tang, W. Liu, et al., "Burdock Fructooligosaccharide Attenuates High Glucose-Induced Apoptosis and Oxidative Stress Injury in Renal Tubular Epithelial Cells," *Frontiers in Pharmacology* 12 (2021): 784187.

[7] L. Ren, C. Perera, and Y. Hemar, "Antitumor Activity of Mushroom Polysaccharides: A Review," *Food & Function* 3 (2012): 1118–1130.

[8] Z. Li, B. Cui, X. Liu, et al., "Virucidal Activity and the Antiviral Mechanism of Acidic Polysaccharides Against Enterovirus 71 Infection In Vitro," *Microbiology and Immunology* 64 (2020): 189–201.

[9] H. Zhu, L. Tian, L. Zhang, et al., "Preparation, Characterization and Antioxidant Activity of Polysaccharide From Spent Lentinus Edodes Substrate," *International Journal of Biological Macromolecules* 112 (2018): 976–984.

[10] Y. Zhang, Z. Zheng, X. Yang, et al., "A Sensitive and Rapid Radiolabelling Method for the *In Vivo* Pharmacokinetic Study of Lentinan," *Food & Function* 9 (2018): 3114–3125.

[11] S. H. Moussa, A. A. Tayel, and A. I. Al-Turki, "Evaluation of Fungal Chitosan as a Biocontrol and Antibacterial Agent Using Fluorescence-Labeling," *International Journal of Biological Macromolecules* 54 (2013): 204–208.

[12] Z. Zheng, X. Pan, J. Xu, Z. Wu, Y. Zhang, and K. Wang, "Advances in Tracking of Polysaccharides *In Vivo*: Labeling Strategies, Potential Factors and Applications Based on Pharmacokinetic Characteristics," *International Journal of Biological Macromolecules* 163 (2020): 1403–1420.

[13] J. Bi, C. Zhao, W. Jin, Q. Chen, B. Fan, and C. Qian, "Study on Pharmacokinetics and Tissue Distribution of *Polygonatum sibiricum* Polysaccharide in Rats by Fluorescence Labeling," *International Journal of Biological Macromolecules* 215 (2022): 541–549.

[14] Q. Huang, Q. Bao, C. Wu, et al., "Carbon Dots Derived From *Poria cocos* Polysaccharide as an Effective "On-Off" Fluorescence Sensor for Chromium (VI) Detection," *Journal of Pharmaceutical Analysis* 12 (2022): 104–112.

[15] Y. Dong, C. Chen, X. Fu, and R. Liu, "Study on the Pharmacokinetics of Mulberry Fruit Polysaccharides Through Fluorescence Labeling," *International Journal of Biological Macromolecules* 186 (2021): 462–471.

[16] W. Dong, B. Han, Y. Feng, et al., "Pharmacokinetics and Biodegradation Mechanisms of a Versatile Carboxymethyl Derivative of Chitosan in Rats: *In Vivo* and *In Vitro* Evaluation," *Biomacromolecules* 11 (2010): 1527–1533.

[17] X. Lin, Z. Wang, G. Sun, L. Shen, D. Xu, and Y. Feng, "A Sensitive and Specific HPGPC-FD Method for the Study of Pharmacokinetics and Tissue Distribution of Radix Ophiopogonis Polysaccharide in Rats," *Biomedical Chromatography* 24 (2010): 820–825.

[18] Y. Kaneo, T. Uemura, T. Tanaka, and S. Kanoh, "Polysaccharides as Drug Carriers: Biodisposition of Fluorescein-Labeled Dextrans in Mice," *Biological and Pharmaceutical Bulletin* 20 (1997): 181–187.

[19] K. Sato, K. Itakura, K. Nishida, Y. Takakura, M. Hashida, and H. Sezaki, "Disposition of a Polymeric Prodrug of Mitomycin C, Mitomycin C-Dextran Conjugate, in the Perfused Rat Liver," *Journal of Pharmaceutical Sciences* 78 (1989): 11–16.

[20] S. Nakane, S. Matsumoto, Y. Takakura, M. Hashida, and H. Sezaki, "The Accumulation Mechanism of Cationic Mitomycin C-Dextran Conjugates in the Liver: *In-Vivo* Cellular Localization and *In-Vitro* Interaction With Hepatocytes," *Journal of Pharmacy and Pharmacology* 40 (1988): 1–6.

[21] T. Tanaka, Y. Fujishima, S. Hamano, and Y. Kaneo, "Cellular Disposition of Arabinogalactan in Primary Cultured Rat Hepatocytes," *European Journal of Pharmaceutical Sciences* 22 (2004): 435–444.

[22] I. W. Kellaway, L. Seale, and P. S. Spencer, "The In Vitro Characterization and Biostability of 99mTc-Dextran and its Accumulation Within the Inflamed Paws of Adjuvant-Induced Arthritic Rats," *Pharmaceutical Research* 12 (1995): 588–593.

[23] R. Mehvar, M. A. Robinson, and J. M. Reynolds, "Dose Dependency of the Kinetics of Dextrans in Rats: Effects of Molecular Weight," *Journal of Pharmaceutical Sciences* 84 (1995): 815–818.

[24] N. N. Miura, N. Ohno, J. Aketagawa, H. Tamura, S. Tanaka, and T. Yadomae, "Blood Clearance of (1--> 3)-Beta-D-Glucan in MRL Lpr/lpr Mice," *FEMS Immunology and Medical Microbiology* 13 (1996): 51–57.

[25] Y. Zhang, Z. Wang, X. Zhang, W. Zhou, and L. Huang, "One-Pot Fluorescent Labeling of Saccharides With Fluorescein-5-Thiosemicarbazide for Imaging Polysaccharides Transported in Living Cells," *Carbohydrate Research* 346 (2011): 2156–2164.

[26] S. Kamoda, M. Nakano, R. Ishikawa, S. Suzuki, and K. Kakehi, "Rapid and Sensitive Screening of N-Glycans as 9-fluorenylmethyl Derivatives by High-Performance Liquid Chromatography: A Method Which Can Recover Free Oligosaccharides After Analysis," *Journal of Proteome Research* 4 (2005): 146–152.

[27] X. Song, Y. Lasanajak, C. Rivera-Marrero, et al., "Generation of a Natural Glycan Microarray Using 9-fluorenylmethyl Chloroformate (FmocCl) as a Cleavable Fluorescent Tag," *Analytical Biochemistry* 395 (2009): 151–160.